Atomic structure and electronic properties of the Si_xSb_{100-x} phase-change memory material

Ashok K. Verma,[1,*] P. Modak,[1] A. Svane,[2] and N. E. Christensen[2]

[1]*High Pressure and Synchrotron Radiation Physics Division, Bhabha Atomic Research Centre, Trombay, Mumbai 400 085, India*

[2]*Dept. of Physics and Astronomy, University of Aarhus, DK 8000, Aarhus C, Denmark*

(Received 15 December 2010; revised manuscript received 17 February 2011; published 20 April 2011)

The electronic and structural properties of Si_xSb_{100-x} ($x\sim16$) materials are investigated using first-principles molecular dynamics simulations. Crystalline-liquid-amorphous phase transitions are examined and remarkable changes in the local structure around the Si atoms are found. The average Si coordination number 6 (3 *long* + 3 *short* Si-Sb *bonds*) of the crystalline phase changes to 4 (3 *long* Si-Sb + 1 *short* Si-Si *bonds*) by preserving three Si-Sb bonds in both the liquid and the amorphous phases. In the amorphous phase ∼90% of the Si atoms are fourfold coordinated compared to 40% in the liquid. The electronic density of states is metal-like in both the crystalline and the liquid phases, but it exhibits a pseudogap at the Fermi level in the amorphous phase, reflecting the strong abundance of fourfold coordinated Si in the amorphous phase.

DOI: 10.1103/PhysRevB.83.134205 PACS number(s): 64.70.dg, 61.20.Gy, 71.15.Mb, 71.15.Pd

I. INTRODUCTION

Most phase-change random access memory (nonvolatile) materials are tellurium-based chalcogenides such as Ge-Sb-Te and Ag-In-Sb-Te systems.[1–3] Te is known to be a toxic and environmentally unfriendly material. Further, Te diffuses into the heating electrode (write or rewrite steps) that may result in degradation of the memory device. Further, Te is not compatible with modern metal-oxide-semiconductor manufacturing units, and machining of these materials is a challenging task that may also lead to compositional changes. Therefore, a simple Te-free binary material is desirable for phase-change random access memory applications.[4–6] Si_xSb_{100-x} is such a system, and it has been investigated experimentally by many researchers. Among several compositions, $Si_{10}Sb_{90}$ and $Si_{16}Sb_{84}$ were found to be especially promising. Samples with these compositions showed better data retention capability and their failure times are 10^3–10^7 times longer than those of the most widely used materials such as $Ge_2Sb_2Te_5$ at temperatures as high as 110 °C. The difference in density between the crystalline and amorphous phases is less than 4% for SiSb, whereas for $Ge_2Sb_2Te_5$ it is much larger, ∼9.5%.[4–6]

Phase-change materials (PCMs) exhibit significant differences in electrical and optical properties when their crystalline and amorphous phases are compared. This makes them suitable for the applications for data storage. The involved phase transformation is ultrafast (a few nanoseconds) and reversible. The crystalline and amorphous phases have very different local atomic arrangements, as also found for the prototype phase-change memory materials (e.g., $GeSb_2Te_4$ and $Ge_2Sb_2Te_5$).[1–3] Therefore, in order to understand the phase-change mechanism and changes in related properties, a detailed knowledge of the local atomic arrangement in both the crystalline and amorphous states is important.

In this work, we report results of pseudopotential density functional theory [within the generalized gradient approximation (GGA)[7]] based molecular dynamics (MD) simulations of the crystalline, liquid, and amorphous phases of SiSb alloys using a 192-atom supercell. A key result is that the local structure around Si atoms differs considerably among the crystal, amorphous, and liquid phases and that the constituent atoms in the amorphous phase to a large extent satisfy the "8−*N*" rule (preference to coordinations which provide a closed shell of eight electrons around each element by sharing electrons with nearest neighbors in covalent bonds),[8,9] where *N* is the number of valence electrons. The liquid-amorphous transformation creates a pseudogap at the Fermi level in the metal-like electronic structure of the amorphous phase, and these electronic structure changes are attributed to the changes in the local structure around the Si atoms. The changes in the electronic properties of crystalline Sb upon Si substitution can be explained by a rigid-band model. Comparative simulations are also performed for pure Sb.

II. METHODS

The first-principles MD simulations in this work are based on finite temperature Mermin density functional theory with the GGA exchange-correlation energy as implemented in the Vienna *ab initio* simulation package[10–13] (VASP). The interactions between core and valence electrons are modeled with the projector augmented plane-wave method, and the Si and Sb pseudopotentials are generated with the $3s^2,3p^2$ and $5s^2,5p^3$ valence configurations, respectively. The MD simulations are carried out in the canonical *NVT* ensemble, and the temperature was controlled using the Nosé thermostat.[14] The simulations are performed with sampling of the (0,0,0) *k* point with a 3-fs time step.

The simulation cell is cubic (17.739 Å edge) with 192 atoms (31 Si + 161 Sb) at a density of $\rho = 6.089$ g/cm^3.[5] Initially, an A7 structure supercell ($4\times4\times2$), constrained to a cube, is generated with 192 Sb atoms, and then 31 Sb atoms were randomly replaced by Si atoms. The simulation cell is heated to 2000 K followed by an equilibration period of 15 ps. The generation of the liquid is confirmed by calculating the radial distribution functions and the mean-square displacements (MSDs) with time. The liquid is then quenched isochorically to room temperature at a rate of 50 K ps^{-1}, followed by an equilibration period of 30 ps. The last 2000 configurations are used for the analysis of the structure and electronic properties. Simulations for pure Sb are also performed by using the same computational parameters.

The electronic densities of states (DOS) are calculated by averaging over several selected atomic configurations for

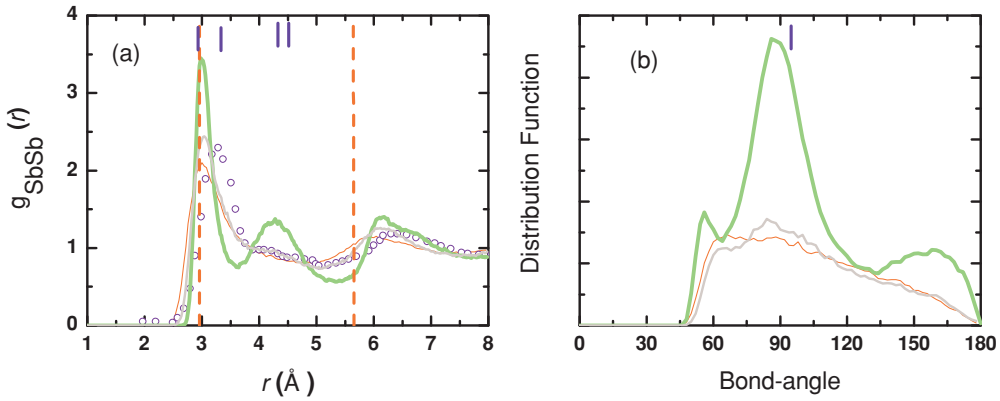

FIG. 1. (Color online) (a) Radial and (b) bond-angle distribution functions of liquid Sb at 2000 K (thin red line), 1000 K (light gray line), and 300 K (thick green line). Vertical bars represent the data of *c*-Sb (A7 structure) and the vertical dashed lines show the first and second peak positions of the simple hard-sphere liquid (Ref. 15). The experimental data taken from Ref. 15 (recorded at $T = 932$ K) is shown with open circles.

the amorphous and liquid phases. However, the DOS for crystalline SiSb is obtained by randomly replacing Sb with Si in an A7 structure supercell with 192 atoms. The Si atoms are placed in such a way that they remain as far as possible from each other. In these DOS calculations a denser *k*-point mesh ($4 \times 4 \times 4$) in the Brillouin zone is employed with a Gaussian broadening of 0.10 eV. The DOS for pure crystalline Sb is calculated in the A7 structure.

III. RESULTS AND DISCUSSION

Since Si_xSb_{100-x} with the composition considered here, $x \sim 16$, is derived from Sb, it is useful to start from pure antimony, and then examine the changes induced by replacing some of the Sb atoms by Si.[6] The structure of liquid Sb differs considerably from that of a simple hard-sphere liquid: The ratio 2.01 of the second (at 5.95 Å) and first (at 2.96 Å) peak positions of the radial distribution function is slightly larger than that of the simple hard-sphere liquid (1.91), and the average coordination number, 6.69, is much smaller than that of the simple hard-sphere liquid (9−11) [Fig. 1(a) and Table I].[15] It is to be noted that antimony is octahedrally (3 + 3) coordinated in the rhombohedral A7 crystal structure. When the liquid is cooled, a new small peak at ∼4.25 Å develops at 1000 K, in agreement with experiments,[15] and at 300 K this peak becomes prominent and its position corresponds to the second-nearest-neighbor distance in the A7 phase. The calculated position of this peak differs slightly from the experimental one due to a density difference ($\rho_{\text{theory}} = 1.05\rho_{\text{expt.}}$). The calculated bond-angle distribution functions are shown in Fig. 1(b). The Sb-Sb-Sb bond-angle distribution in the amorphous phase has a prominent peak at 89.3°, close to that in the A7 structure (∼93.3°). Other peaks are located at ∼60° and 120°. Thus, the bonding characteristics in crystalline and amorphous Sb phases are rather similar, i.e., the Sb-Sb covalent bonds of the crystalline phase survive not only in the amorphous phase but also in the liquid, even at 1000 K. Other covalent liquids such as Si, Ge, and As are also known to show such structural changes in the supercooled state.[16,17]

TABLE I. Bond lengths ($R_{\alpha-\beta}$) and coordination numbers ($Z_{\alpha-\beta}$) in the liquid and amorphous states. Sb-Sb, Si-Si, and Sb-Si cutoff distances (R_C) were taken as 3.60, 2.68, and 3.04 Å, respectively, for both the liquid and amorphous states. The average cutoff distance was also taken to be 3.60 Å for the tot-tot case.

	Pair	$R_{\alpha-\beta}$ (Å)	$Z_{\alpha-\beta}$ (R_C)
l-SiSb	tot-tot	2.96	6.45
	Sb-Sb	3.04	5.33
	Si-Si	2.38	0.92
	Sb-Si	2.68	0.57
	Si-Sb	2.68	2.99
a-SiSb	tot-tot	2.95	5.61
	Sb-Sb	2.95	4.83
	Si-Si	2.36	1.21
	Sb-Si	2.62	0.55
	Si-Sb	2.62	2.86
c-SiSb	Si-Sb	2.70−3.60	3 + 3
l-Sb	Sb-Sb	3.00	6.69
a-Sb	Sb-Sb	2.98	6.22

The overall structure of liquid $Si_{16}Sb_{84}$ is similar to that of liquid Sb: The shape of the total radial distribution function and the average coordination numbers are nearly identical [see Fig. 2(a) and Table I]. Analysis of the partial radial distribution functions [Figs. 2(b)−2(d)] reveals that the first neighbor pairs in liquid SiSb are composed of Sb-Sb, Si-Si, and Sb-Si pairs with peaks in the radial distribution function corresponding to 3.04, 2.38, and 2.68 Å, respectively. The average Sb-Sb, Si-Si, Sb-Si, and Si-Sb coordination numbers are 5.33, 0.92, 0.57, and 2.99, respectively.

The calculated mean-square distribution (MSD) functions of Si and Sb atoms grow linearly with time as expected for liquids (Fig. 3). The slope of the MSD is used to estimate the respective diffusion constants, and it is found that the Si atoms diffuse much faster than the Sb atoms (∼16 times). The self-diffusion constant of Sb in pure Sb liquid and in SiSb liquid are comparable. The calculated self-diffusion constants of Si and Sb in the liquid SiSb are in good agreement with available literature values as given in Table II.[18,19]

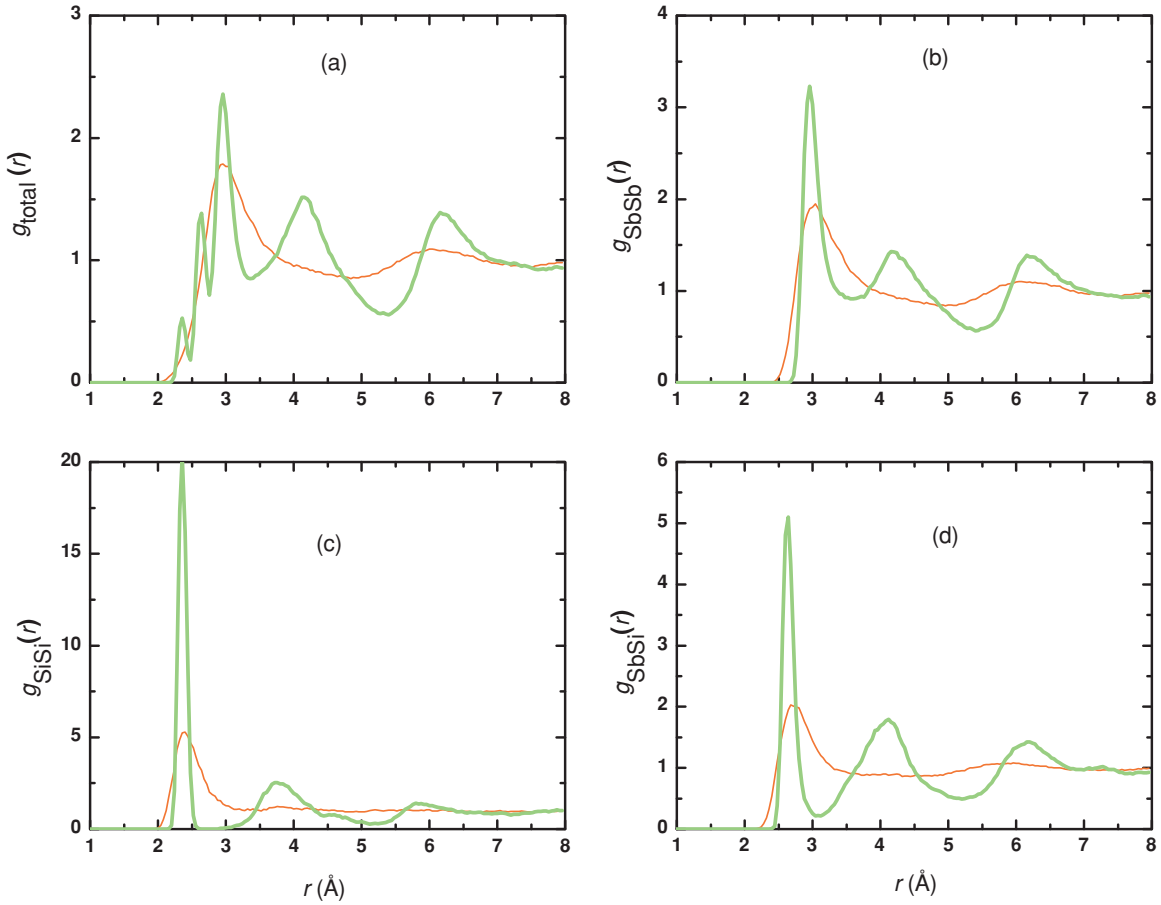

FIG. 2. (Color online) Calculated radial distribution functions of the liquid (thin red lines) and amorphous (thick green lines) phases of $Si_{16}Sb_{84}$. The total distribution function is shown in (a), while the partial Sb-Sb, Si-Si and Sb-Si distribution functions are shown in (b), (c), and (d), respectively.

Large structural modifications take place when the liquid is quenched to room temperature: The first peak of the total radial distribution function splits into three sharper peaks, which are located at 2.36, 2.62, and 2.95 Å, respectively [Fig. 2(a)]. The partial radial distribution functions show that these peaks are primarily related to Si-Si (*first peak*), Sb-Si (*second peak*), and Sb-Sb pairs (*third peak*). Two other peaks which are located at 4.22 and 6.26 Å have contributions from all possible types of pairs [Fig. 2(a)]. Although the average Sb-Si coordination number remains nearly unchanged during the liquid-to-amorphous transition, there are noticeable changes in other coordination numbers. For example, the average Si-Si coordination number increases by $\sim$ 32%, and the Sb-Sb and Si-Sb coordination numbers decrease by $\sim$ 9 and 4%, respectively (Table I).

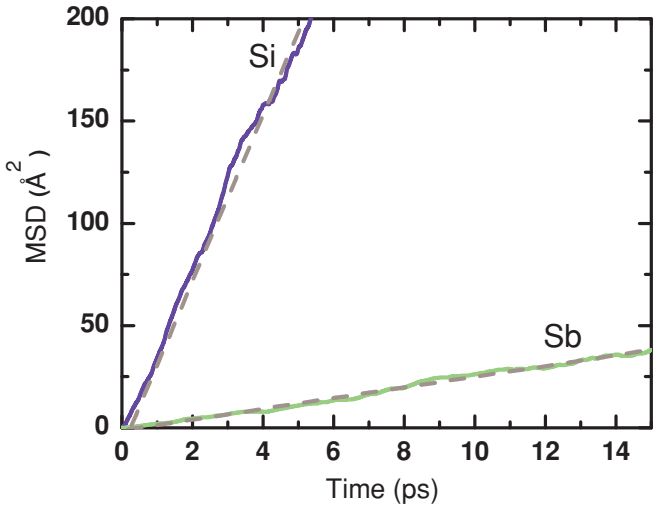

FIG. 3. (Color online) Calculated MSD of Si and Sb atoms in liquid $Si_{16}Sb_{84}$ with time at 2000 K. The dashed lines are linear fits to the MSD data.

TABLE II. Calculated self-diffusion constants of Si and Sb in liquid $Si_{16}Sb_{84}$ at 2000 K. The data inside the parentheses are taken from the previous first-principles simulations (Refs. 18 and 19). For Si (Ref. 18) it is for pure liquid Si at 1800 K, whereas that for Sb (Ref. 19) is in $Ge_2Sb_2Te_5$ at 1000 K.

		Diffusion constants ($\times 10^{-4}$ cm^2 s^{-1})
(*l*-SiSb)	Si	6.77 (2.26)
	Sb	0.43 (0.47)
(*l*-Sb)	Sb	0.36

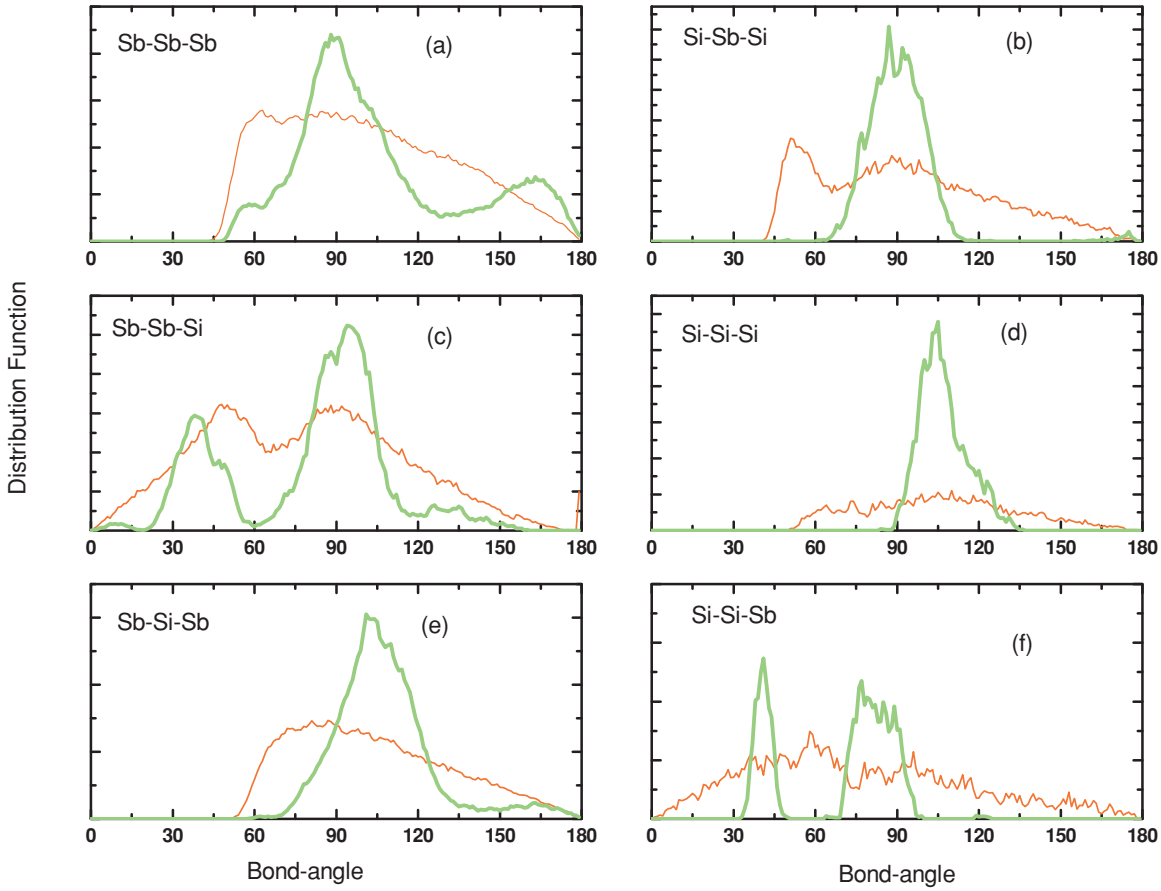

FIG. 4. (Color online) Calculated bond-angle distribution functions of the liquid (thin red lines) and amorphous (thick green lines) phases of $Si_{16}Sb_{84}$. (a) Sb-Sb-Sb angles, (b) Si-Sb-Si angles, (c) Sb-Sb-Si angles, (d) Si-Si-Si angles, (e) Sb-Si-Sb angles, (f) Si-Si-Sb angles.

The bonds are expected to be flexible in the liquid, and their flexibility emerges nicely in the bond-angle distributions plots (see Fig. 4). The Si-Sb-Si bond-angle distribution [Fig. 4(b)] has peaks at $\theta \sim 52^\circ$ (*sharp*) and $\theta \sim 90^\circ$ (*broad*) and Sb-Sb-Si bond-angle distribution [Fig. 4(c)] has peaks at $\theta \sim 40^\circ$ and $\theta \sim 90^\circ$. The distribution functions shown in Figs. 4(a), 4(d), and 4(e) look very similar in nature, having a humplike feature with appreciable weights between angles $\theta \sim 55^\circ - 150^\circ$, whereas the distribution function shown in Fig. 4(f) has weight over all angles. However, the bond-angle distributions develop sharp peaks, similar to the radial distribution functions, upon cooling to room temperature, which is an indication of their rigidity against deformations. Now the Sb-Si-Sb and Si-Si-Si [Figs. 4(d) and 4(e)] bond-angle distributions develop peaks at $\theta \sim 103^\circ$ and $\theta \sim 105^\circ$, respectively. The Sb-Si-Si distribution develops peaks at $\theta \sim 40^\circ$ and $\theta \sim 80^\circ$. However, all Sb centered bond-angle distributions [Figs. 4(a)–4(c)] have their most prominent peak at $\theta \sim 90^\circ$. The Sb-Sb-Sb bond-angle distribution, similar to the amorphous Sb, has two additional peaks at $\theta \sim 55^\circ$ (*smallest*) and 166° (*broad*). Therefore, it is expected that Sb and Si will have predominant *p*- and sp^3-type bonding, respectively, in the amorphous phase, as bond angles for pure *p*- and sp^3-hybridized bonds are 90° and 109.47°, respectively.

The average Si coordination number (∼4) is almost the same in the liquid and in amorphous SiSb, but the distribution of Si coordinations shows a remarkable change during the liquid-amorphous transformation [Fig. 5(a)]. The fourfold coordinated Si fraction is significantly increased in the amorphous phase (∼2.25 times that of the liquid): ∼90% of the Si atoms are fourfold coordinated. This is an unusually large fraction of fourfold coordinated atoms for any PCM.[1] In Te-based PCM materials such as $Ge_2Sb_2Te_5$ and GeTe only 60% Ge atoms are reported to exist in the fourfold coordinated environment.[19,20] Si in the SiSb liquid is primarily two- (10%), three- (42%), four- (36%), and six- (10%) fold coordinated. The populations of Sb coordinations (especially higher) also showed changes during amorphization. In the amorphous phase of $Si_{16}Sb_{84}$, Sb is mostly four- (12%), five- (40%), and six- (38%) fold coordinated, whereas in the liquid phase Sb is mostly five- (27%), six- (37%), and seven- (16%) fold coordinated. Similar trends are also seen in the pure Sb during amorphization [Fig. 5(b)]. However, a marked change (∼1.5 times increase) in the sixfold coordination occurs during the liquid to the amorphous transition in the pure Sb.

Figure 5(c) illustrates the sixfold coordinated local structure of Si atoms in the crystal and Figs. 5(d)–5(f) illustrate all possible fourfold coordinated local structures of Si atoms as obtained in the amorphous phase. Figure 6 shows the time evolution of the average local structure around Si and Sb atoms during the liquid-amorphous transition, as obtained in our simulations. In the liquid phase the average local

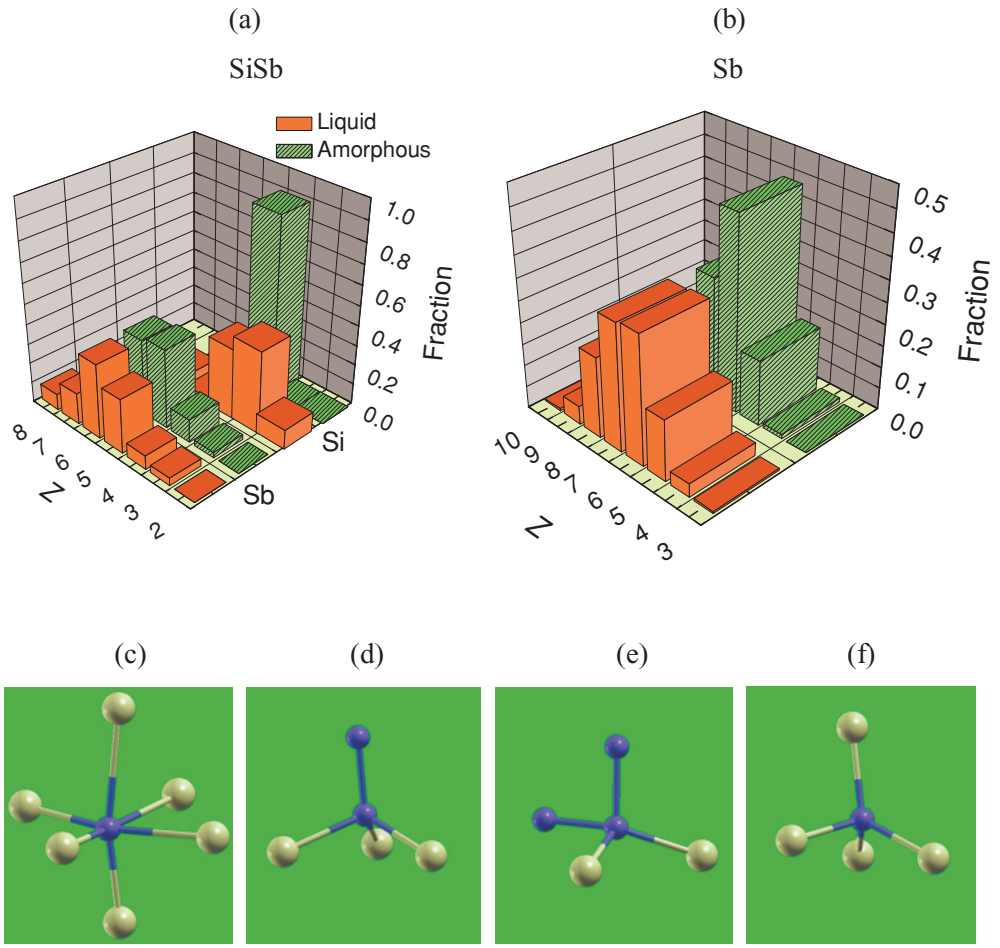

FIG. 5. (Color online) (a) Distribution of different coordination numbers around Si and Sb in amorphous $Si_{16}Sb_{84}$ and (b) distribution of different coordination numbers in amorphous Sb. The lower panel illustrates typical local environments around Si in the crystalline (c) and amorphous phases (d)−(f) of $Si_{16}Sb_{84}$. Large yellow spheres represent Sb atoms and small blue spheres represent Si atoms.

structure around each atom type is weakly defined as there are larger fluctuations in the average nearest-neighbor distances around both Si and Sb atoms. However, a marked change in average local structure around Si atoms is seen during the amorphization as a gap has opened up between fourth- and fifth-nearest-neighbor distances. A small change is also seen between the fifth and sixth neighbor distances around the Sb atom during amorphization. This clearly shows that the shortest three bonds of the crystal, with an average bond length 2.7 Å, are preserved during crystal-liquid-amorphous transitions in this compound. Thus the assumption of similarity of the local structures (i.e., first three neighbors of Si) in the crystalline and amorphous states of a random covalent network model for glass seems reasonable for the SiSb system; three shorter (*stronger*) Si-Sb bonds of the crystalline phase are preserved in the amorphous phase, although the average coordination number changes considerably due to rupture of the weaker bonds (found in the crystal) during the amorphization process.[21] This structural similarity between the crystalline and amorphous phases may be causing the high crystallization speed which is desirable for rapid switching (also supported by ring analysis—see below). On the other hand, broken bonds, which result in destruction of long-range order, may lead to differences in the electrical and optical properties of the two phases. However, it is worth mentioning that recently the optical and electrical contrast between the crystalline and amorphous phases has been explained in terms of resonant bonding.[22,23]

From the above analysis it is clear that the coordination numbers of Si (∼4) and Sb (∼5) in the amorphous phase obey the $8-N$ rule,[8,9] which is different from the Te-based PCM materials such as $Ge_2Sb_2Te_5$ and GeTe, where large deviations from the $8-N$ rule were seen for both systems.[19,20] For Si, its four valence electrons participate in bonding via sp^3 hybridization, whereas for Sb usually its three $5p$ electrons participate in the bonding. However, in the liquid phase both Sb and Si are in the sixfold coordinated environment.

A ring structure analysis using the King's criterion[24] (Fig. 7) shows both even- and odd-numbered rings for amorphous SiSb because of the homopolar nature of the bonds, such as Si-Si and Sb-Sb bonds, in contrast to the well-known PCM, Ge-Sb-Te, for which a strong preference for even-numbered ring structures was found in the amorphous phase.[25] The amorphous phase has three- (15.2%), four- (48.8%), and five- (35.5%) fold rings. Analysis of crystalline SiSb shows that it only contains fourfold rings. Dominance of fourfold rings in

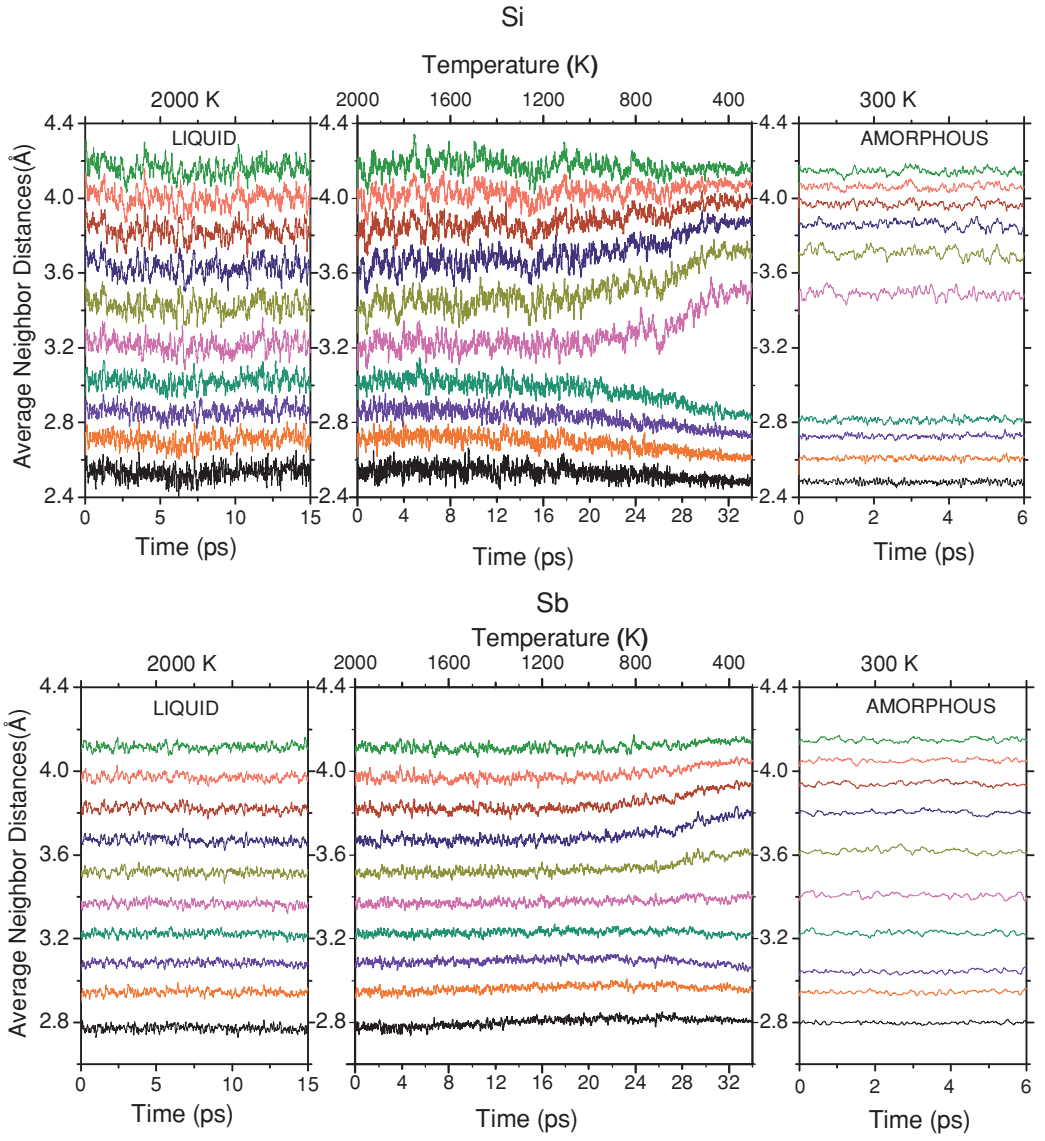

FIG. 6. (Color online) Time evolution of the average nearest-neighbor distances around Si and Sb atoms in the liquid phase, during liquid-amorphous transition, and in the amorphous phase. The first ten nearest-neighbor distances around Si and Sb atoms are shown. The average nearest neighbor distances evolution in the liquid phase at 2000 K and that in the amorphous phase at 300 K are given for reference.

the amorphous phase may result in faster crystallization speed, as pointed out in Ref. 26.

Since the crystal-liquid-amorphous transformations in the SiSb system are associated with large structural changes, it is

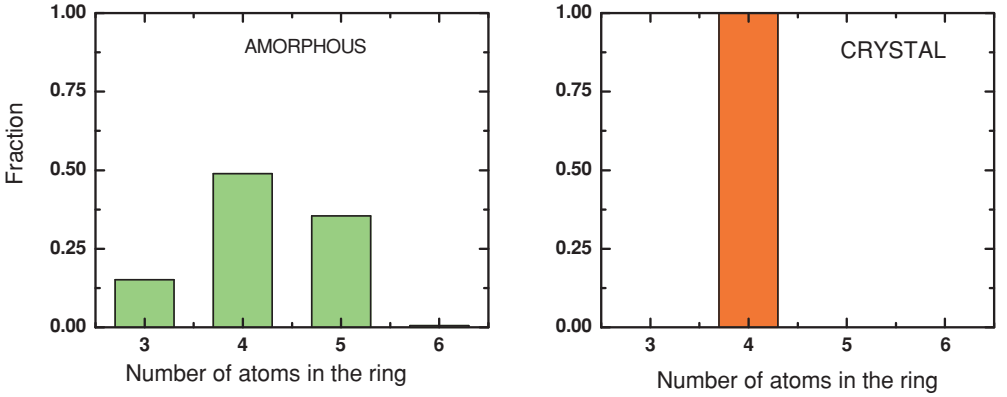

FIG. 7. (Color online) Distribution of shortest path King's rings (Ref. 24) in amorphous and crystalline $Si_{16}Sb_{84}$. In the ring analysis of the amorphous phase Sb-Sb, Si-Si, and Sb-Si cutoff distances were taken as 3.60, 2.68, and 3.04 Å, respectively.

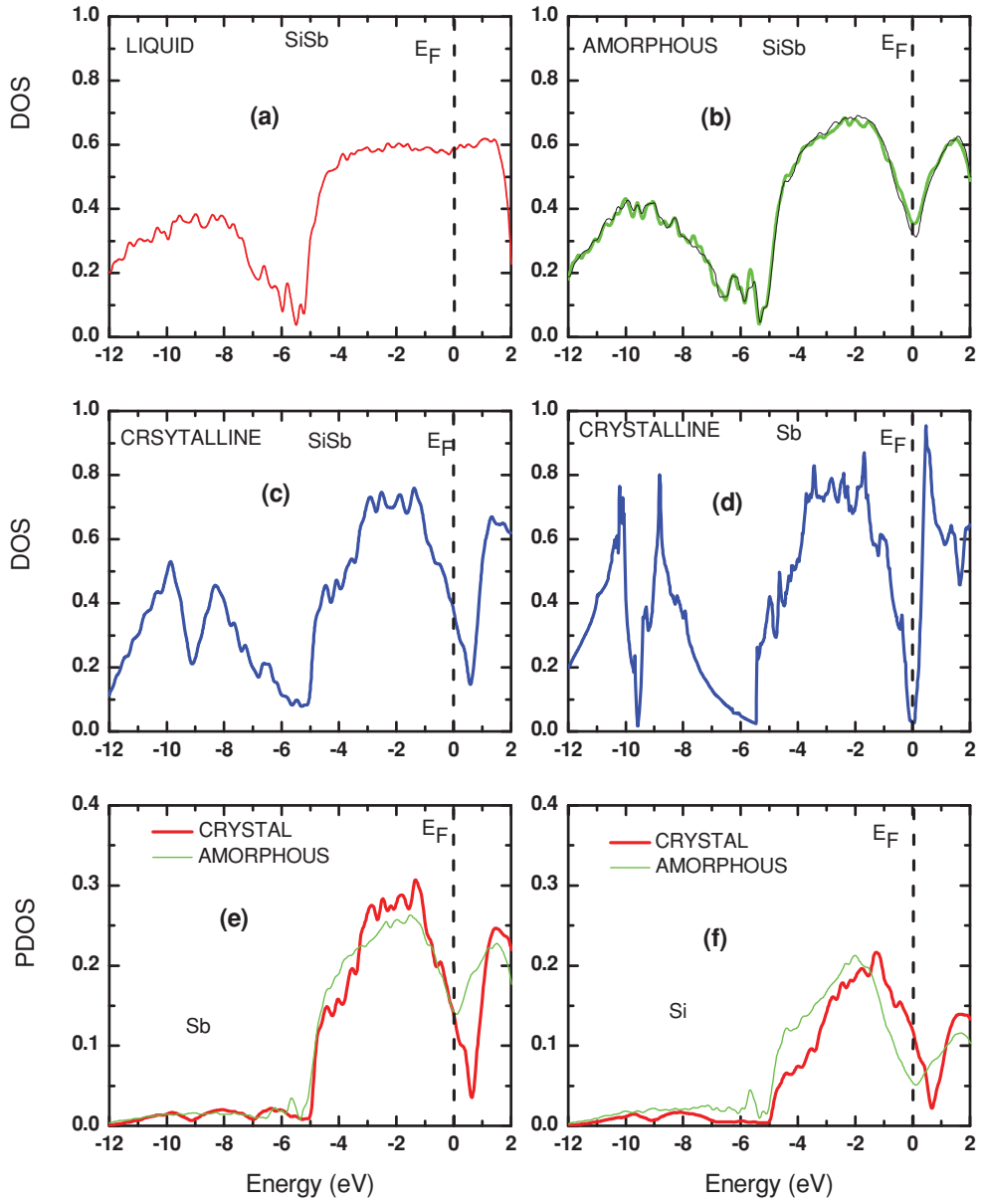

FIG. 8. (Color online) Electronic DOS (states eV^{-1} $atom^{-1}$) of the (a) liquid, (b) amorphous, and (c) crystalline phases of SiSb. Bottom panels (e) and (f) show the Sb and Si atom projected *p*-orbital DOS for the crystalline and amorphous SiSb phases. For reference, the DOS of crystalline Sb in the A7 structure is shown in (d). The DOS of one of the force minimized configurations (thin black line) of amorphous SiSb is also shown in (b).

interesting to study their effects on the electronic structure as represented by the DOS functions. Figure 8 shows the DOS functions calculated for the three SiSb phases. The DOS of the liquid and amorphous phases were calculated as averages over several selected atomic configurations. The DOS of the crystalline $Si_{16}Sb_{84}$ was calculated by using a 192-atom A7 structure-based supercell with a random substitution of 31 Sb atoms by Si, with a subsequent relaxation of all atomic coordinates by Hellman-Feynman force minimization. During Si substitutions care was taken that they stayed as far as possible from each other (avoiding clustering).

The electronic structure of the liquid is metal-like [Fig. 8(a)], and the value of the electronic DOS at the Fermi level is 0.59 states eV^{-1} $atom^{-1}$ which is close to the free-electron value of 0.68 eV^{-1} $atom^{-1}$. A remarkable change in the DOS is seen when the liquid is quenched to the amorphous phase: The metal-like liquid electronic DOS develops a pseudogap at the Fermi level [Fig. 8(b)]. However, the amorphous Si_xSb_{100-x} ($x = 4$, 10, 16, and 32) systems are known to be semiconductors whose band gaps lie between 0.41 and 0.50 eV.[6] Although the value of the DOS at the Fermi level decreases slightly for the relaxed configuration (in the amorphous phase), it failed to open a gap at the Fermi level as observed in experiments.[4–6] Geometrical disorder is known to produce a narrow band of localized states which are not treated well by density functional theory in the present form

[local density approximation (LDA) and GGA[7] which is more suited to treat delocalized states.[27] Band-gap underestimations are also typical of LDA- and GGA-based calculations even for simple *sp* systems.[28,29] More accurate descriptions of localized states and of band gaps are possible with many-body methods such as *GW* approximations.[28–31] However, such calculations are still computationally impossible for cases involving large supercells.

The shape of the DOS of crystalline SiSb is very much like that of crystalline Sb, but the position of the Fermi level is quite different. Unlike Sb, the Fermi level for $Si_{16}Sb_{84}$ is not in the middle of the pseudogap; it is shifted by 0.60 eV toward lower energies, away from the middle of the gap. In $Si_{16}Sb_{84}$, the value of the DOS at the Fermi level is ~ 12 times higher than that in Sb. The Fermi-level shift and the DOS increase can be understood from a simple rigid-band model. Since Si has one valence electron less than Sb, replacement of Sb by Si corresponds to hole doping of antimony. This causes the Fermi level to move down in energy, where the DOS value is higher.

An analysis of the Si- and Sb-atom projected partial DOS [Figs. 8(e) and 8(f)] shows that the uppermost valence band stems from *p* orbitals alone. These are very sensitive not only to coordination numbers but also to bond angles. The intensities of *p*-orbital contributions for octahedral (*crystalline*) and tetrahedral (*amorphous* and *liquid*) Si reflect the amount of band overlap which can be related to bond strength. Stronger bonds are expected to be related to wider bands and vice versa. From Figs. 8(e) and 8(f), the most marked difference between the atom-projected DOS functions of the crystalline and amorphous $Si_{16}Sb_{84}$ is the reduction of the Si DOS at the Fermi level in the amorphous phase, while the Sb contribution is very similar for the crystalline and amorphous phases.

IV. CONCLUSIONS

First-principles molecular dynamics simulations of Si_xSb_{100-x} ($x \sim 16$) phase-change memory alloys have been presented. These simulations reveal unique properties of the SiSb materials which are important for data storage applications. They show that these properties result from changes in the local structure around Si during the amorphization: 6-cordination changes into 4-coordination. Fast crystallization, which is essential to applications since it means short switching times, is expected because only three weaker bonds are broken, but the remaining three stronger bonds in the crystalline phase are not affected by the amorphization. Fast crystallization is further supported by ring analysis as fourfold rings are prevalent in both the crystalline and the amorphous phases. This material is expected to be superior to commonly used PCM materials against void formation and degradations in repeated cycles of operations because of the small volume change in the crystalline-to-amorphous phase transition.

*hpps@barc.gov.in

[1] M. Wuttig and N. Yamada, Nat. Mater. **6**, 824 (2007).
[2] A. Klein, H. Dieker, B. Späth, P. Fons, A. Kolobov, C. Steimer, and M. Wuttig, Phys. Rev. Lett. **100**, 016402 (2008).
[3] M. Xu, Y. Q. Cheng, H. W. Sheng, and E. Ma, Phys. Rev. Lett. **103**, 195502 (2009).
[4] T. Zhang, Z. T. Song, F. Wang, B. Liu, S. L. Feng, and B. Chen, Jpn. J. Appl. Phys., Part 2 **46**, L602 (2007).
[5] T. Zhang, Z. T. Song, F. Wang, B. Liu, S. L. Feng, and B. Chen, Appl. Phys. Lett. **91**, 222102 (2007).
[6] T. Zhang, Z. T. Song, F. Wang, B. Liu, S. L. Feng, and B. Chen, Semicond. Sci. Technol. **23**, 055010 (2008).
[7] J. P. Perdew, K. Burke, and M. Ernzerhof, Phys. Rev. Lett. **77**, 3865 (1996).
[8] N. F. Mott, Adv. Phys. **16**, 49 (1967).
[9] N. E. Christensen, S. Satpathy, and Z. Pawlowska, Phys. Rev. B **36**, 1032 (1987).
[10] G. Kresse and J. Hafner, J. Phys. Condens. Matter **6**, 8245 (1994).
[11] G. Kresse and J. Furthmüller, Comput. Mater. Sci. **6**, 15 (1996).
[12] P. E. Blöchl, Phys. Rev. B **50**, 17953 (1994).
[13] G. Kresse and D. Joubert, Phys. Rev. B **59**, 1758 (1999).
[14] S. Nosé, Mol. Phys. **52**, 255 (1984).
[15] Y. Waseda, *The Structure of Noncrystalline Materials* (McGraw-Hill, New York, 1980).
[16] S. Ansell, S. Krishnan, J. Felton, and D. L. Price, J. Phys.: Condens. Matter **10**, L73 (1998).
[17] G. Kresse and J. Hafner, Phys. Rev. B **49**, 14251 (1994).
[18] I. Stich, R. Car, and M. Parrinello, Phys. Rev. B **44**, 4262 (1991).
[19] J. Akola and R. O. Jones, Phys. Rev. B **76**, 235201 (2007).
[20] S. Caravati, M. Bernasconi, T. D. Kühne, M. Krack, and M. Parinello, Appl. Phys. Lett. **91**, 171906 (2007).
[21] W. Zachariasen, J. Am. Chem. Soc. **54**, 3841 (1932).
[22] K. Shportko, S. Kremers, M. Woda, D. Lencer, and J. M. Wuttig, Nat. Mater. **7**, 653 (2008).
[23] B. Huang and J. Robertson, Phys. Rev. B **81**, 081204 (2010).
[24] S. V. King, Nature (London) **213** 1112 (1967).
[25] S. Kohara, K. Kato, S. Kimura, H. Tanaka, T. Usuki, K. Suzuya, H. Tanaka, Y. Moritomo, T. Matsunaga, N. Yamada, Y. Tanaka, H. Suematsu, and M. Takata, Appl. Phys. Lett. **89**, 201910 (2006).
[26] J. Hegedüs and S. R. Elliott, Nature (London) **7** 399 (2008).
[27] E. A. Davis and N. F. Mott, Philos. Mag. **22**, 903 (1970).
[28] L. Hedin, Phys. Rev. **139**, A7 96 (1965).
[29] M. S. Hybertsen and S. G. Louie, Phys. Rev. Lett. **55**, 1418 (1985).
[30] F. Aryasetiawan and O. Gunnarsson, Rep. Prog. Phys. **61**, 237 (1998).
[31] P. Modak, A. Svane, N. E. Christensen, T. Kotani, and M. van Schilfgaarde, Phys. Rev. B **79**, 153203 (2009).